IEEE Photonics Journal
An IEEE Photonics Society Publication



# A Compact Low-Power 320-Gb/s WDM Transmitter Based on Silicon Microrings

Volume 6, Number 3, June 2014

**Ran Ding**
**Yang Liu**
**Qi Li**
**Zhe Xuan**
**Yangjin Ma**
**Yisu Yang**
**Andy Eu-Jin Lim**
**Guo-Qiang Lo**
**Keren Bergman**
**Tom Baehr-Jones**
**Michael Hochberg**

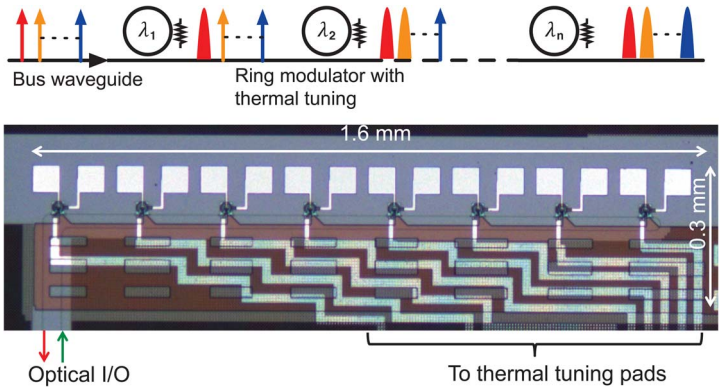


DOI: 10.1109/JPHOT.2014.2326656
1943-0655 © 2014 IEEE

# A Compact Low-Power 320-Gb/s WDM Transmitter Based on Silicon Microrings

**Ran Ding,[1] Yang Liu,[1] Qi Li,[2] Zhe Xuan,[1] Yangjin Ma,[1] Yisu Yang,[1] Andy Eu-Jin Lim,[3] Guo-Qiang Lo,[3] Keren Bergman,[2] Tom Baehr-Jones,[1] and Michael Hochberg[1,3,4]**

[1]Department of Electrical and Computer Engineering, University of Delaware, Newark, DE 19716 USA
[2]Department of Electrical Engineering, Columbia University, New York, NY 10027 USA
[3]Agency for Science, Technology and Research, Institute of Microelectronics, Singapore 138632
[4]Department of Electrical and Computer Engineering, University of Singapore, Singapore 117576

*DOI: 10.1109/JPHOT.2014.2326656*


Manuscript received April 8, 2014; revised May 12, 2014; accepted May 15, 2014. Date of publication May 23, 2014; date of current version June 3, 2014. This work was supported by the AFOSR STTR under Grants FA9550-12-C-0079 and FA9550-12-C-0038, by the NRF Fellowship under Grant NRF2012NRF-NRFF001-143, by the PECASE under Award FA9550-13-1-0027, by the ongoing funding for OpSIS under Grant FA9550-10-1-0439, and by Portage Bay Photonics, LLC. R. Ding and Y. Liu contributed equally to this work. Corresponding author: R. Ding (e-mail: dingran@udel.edu).

**Abstract:** We demonstrate a compact and low-power wavelength-division multiplexing transmitter near a 1550-nm wavelength using silicon microrings. The transmitter is implemented on a silicon-on-insulator photonics platform with a compact footprint of 0.5 $mm^2$. The transmitter incorporates 8 wavelength channels with 200-GHz spacing. Each channel achieved error-free operation at 40 Gb/s, resulting in an aggregated data transmission capability of 320 Gb/s. To our knowledge, this is the highest aggregated data rate demonstrated in silicon wavelength-division multiplexing transmitters. Owing to the small device capacitance and the efficient pn-junction modulator design, the transmitter achieves low energy-per-bit values of 36 fJ/bit under 2.4 $V_{pp}$ drive and 144 fJ/bit under 4.8 $V_{pp}$ drive. Comparisons are made to a commercial lithium niobate modulator in terms of bit-error-rate versus optical signal-to-noise ratio.

**Index Terms:** Integrated optics devices, modulators, integrated optoelectronic circuits.

## 1. Introduction

Silicon photonics offers promising solutions to the demand of increasingly higher data transmission capacity in applications ranging from short-reach optical interconnects [1] to long-haul telecommunications [2]. Wavelength-division multiplexing (WDM) system has attracted more and more interests in the past several years for building high capacity optical network and optical interconnects. Compared to other transmission schemes to aggregate more data rate on to one fiber channel, WDM offers a good tradeoff between systems complexity, electronics overhead and overall data throughput.

In silicon platforms, Mach-Zehnder based modulators have been employed to implement WDM transmitters, in which a wavelength multiplexer is needed to combine different wavelength channels into one output [3]–[5]. An alternative approach is to use microring modulators [6], which can offer significantly smaller footprint and lower power consumption compared to Mach-Zehnder modulators. Furthermore, ring resonator structures are wavelength-selective, allowing them to operate at a set of wavelength channels with little cross-talk to each other. This in effect integrates the

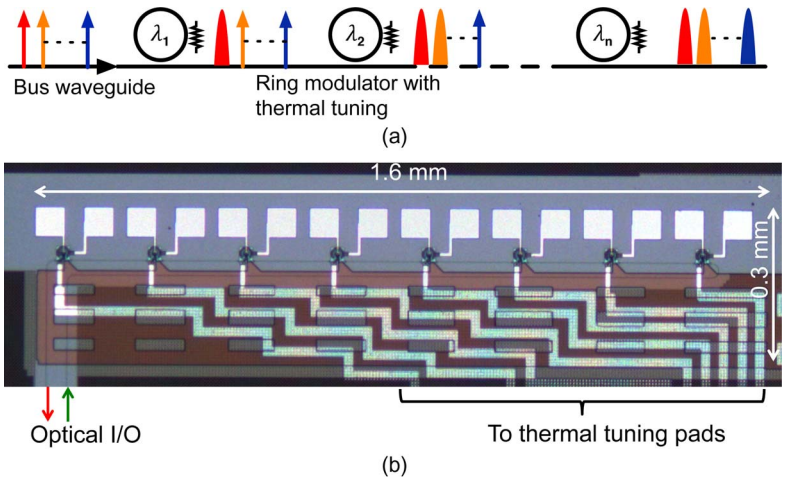


Fig. 1. WDM ring transmitter. (a) Architecture diagram. (b) Chip photo.

wavelength multiplexing function into the ring device itself. This feature is particularly suitable for WDM operation in both transmitters and receivers [7], [8].

The WDM ring transmitter architecture studied in this work is illustrated in Fig. 1(a): a series of ring modulators are coupled to a common bus waveguide and the bus waveguide is connected to the optical input and output of the WDM transmitter. All the laser wavelengths utilized in the transmitter are present on this bus waveguide, while each ring modulator selectively modulates only the wavelength that its resonance is aligned to. The multiple laser wavelengths can come from a comb laser source [9] or multiple single-wavelength lasers pre-multiplexed together [10]. One key design consideration with ring modulators is that its resonance wavelength is sensitive to fabrication and temperature variations. The sensitivity is approximately 0.5-nm resonance shift per 0.5-nm device dimensional change [11] and 80 pm/°C [12], respectively. Therefore, a key requirement on the ring modulators is that they can be tuned to compensate for such resonance drift, so that the resonance can be aligned with the WDM wavelength grid. This is a feature lacking in early work in silicon WDM ring transmitters [13]–[15]. In this paper,we present an $8 \times 40$ Gb/s WDM transmitter using thermally tunable silicon microring modulators. To the best of our knowledge this demonstrates the highest aggregated data transmission capability in silicon WDM transmitters, and is a significant improvement over prior art [8], [10], [13]–[16] in terms of channel rate as well as aggregated throughput. Owing to the high modulation efficiency of the modulators at 40 Gb/s, we demonstrate 36 fJ/bit modulation power efficiency under 2.4 $V_{pp}$ drive and 144 fJ/bit under 4.8 $V_{pp}$ drive. The core devices and metal wiring occupy less than 0.5 $mm^2$ chip area, as shown in Fig. 1(b), while the ring modulators themselves have a much more miniaturized footprint, offering the possibility of large-scale dense integration.

## 2. Ring Modulator Design and Characterization

The key element in the transmitter is the thermally tunable ring modulators. The ring modulators are formed by ridge waveguide of 500-nm width, 90-nm slab height and 7.5 $\mu$m radius resulting a free spectral range (FSR) of 12.8 nm. Approximately 75% of the waveguide was doped with pn junction for high-speed modulation as shown in Fig. 2(a). As illustrated in the cross-section view in Fig. 2(b), the pn junction is formed in the center of waveguide with doping level near $2 \times 10^{18}$ $cm^{-3}$. The ring-to-bus coupling region is doped n-type forming a resistor of 550 $\Omega$ for thermal tuning. The WDM transmitter reported here was fabricated at the Institute of Microelectronics (IME), A*STAR, Singapore, through an OpSIS multi-project-wafer run [17]. The fabrication process enables monolithic integration of both modulators and photodetectors [18], therefore it is straightforward to incorporate the designed modulator in building larger systems [19].

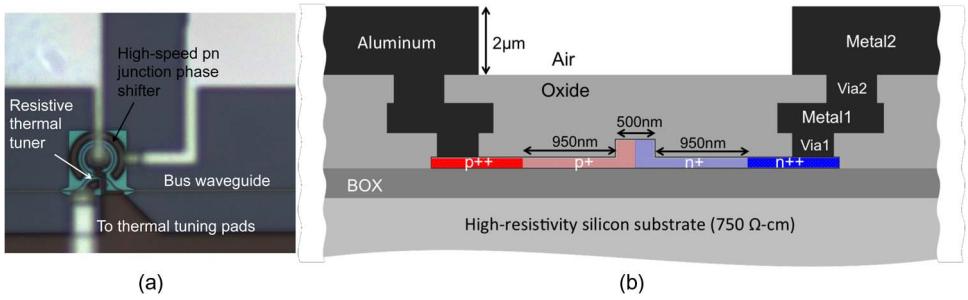


Fig. 2. Ring modulator. (a) Device photo. (b) Phase-shifter cross-section diagram.

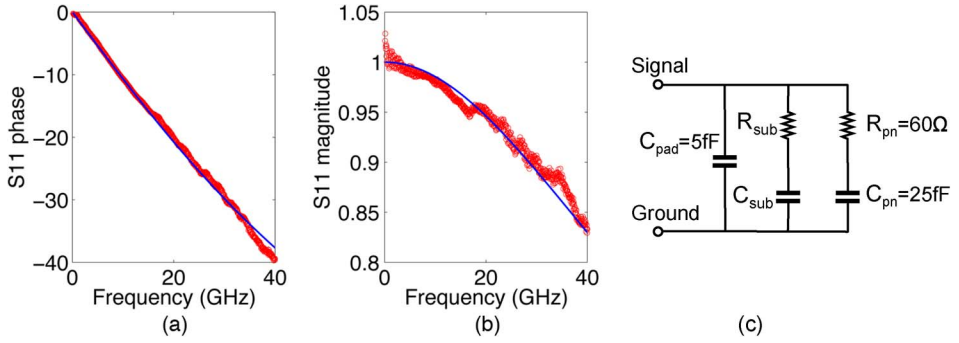


Fig. 3. Ring modulator circuit model parameter extraction based on S11 fitting. (a) S11 phase fit. (b) S11 magnitude fit. (c) Circuit model with extracted parameters.

The high-speed portion of the ring modulator can be viewed as a simple RC circuit, as shown in Fig. 3(c). $C_{pad}$ represents the fringing capacitance between the signal and the ground pad. The branch of $R_{pn}$ and $C_{pn}$ is the key signal path, where $C_{pn}$ is the junction capacitance and $R_{pn}$ is the series silicon resistance from the electrodes to the pn junction. The branch of substrate resistance $R_{sub}$ and device-to-substrate capacitance $C_{sub}$ represents the electrical path from the signal pad through the substrate to the ground pad. By fitting RF S11 parameter of the device [Fig. 3(a) and (b)] we extracted that $C_{pad}$ is 5 fF, $C_{pn}$ is 25 fF and $R_{pn}$ is 60 $\Omega$. Owing to the high resistivity of the silicon substrate (750 $\Omega$-cm), the branch of $R_{sub}$ and $C_{sub}$ presents more than a factor of 10 higher impedance than the branch of $R_{pn}$ and $C_{pn}$ in the frequency range of interest. Therefore, $R_{sub}$ and $C_{sub}$ have little effect in the frequency response of the device and are omitted in the fitting model. Based on the extracted circuit model, we calculated that when the ring modulator is connected with a 50 $\Omega$ source, from the input to $C_{pn}$, an electrical 3-dB bandwidth of approximately 50 GHz is supported.

The optical modulation efficiency is largely determined by the resonator quality factor Q and the tunability of the pn junction. Given the wide RC bandwidth, we choose the Q to be 5,000 providing optical bandwidth of 25 GHz [20], sufficient to support 40 Gb/s operation. The ring modulator pn junction tunability $(\mathrm{d}\lambda/\mathrm{d}V)$ is measured to be 25 pm/V near 0 V bias, as shown in Fig. 4. The phase shifter modulation efficiency in terms of $V_\pi L$ is 1.23 V-cm, calculated using $V_\pi L = (\lambda^2/2n_g) \times (1/(\mathrm{d}\lambda/\mathrm{d}V))$. Using the resistive heater mentioned earlier, the ring resonance can be thermally tuned to compensate for fabrication and temperature variations. The thermal tunability is measured to be 217 pm/mW (i.e., 59 mW/FSR) implying an thermal resistance of 2.8 °C/mW.

The small-signal electro-optical (EO) modulation bandwidth was characterized by S-parameter measurements, using a 67-GHz bandwidth vector-network-analyzer (VNA) and a 70-GHz bandwidth photodetector. The device is probed using a standard 40-GHz rated GS RF probe. The pn junction is biased at 0 V. The EO bandwidth of microring is highly dependent on the wavelength offset from the resonance [21], [22]. We chose to report the EO S21 bandwidth when the output

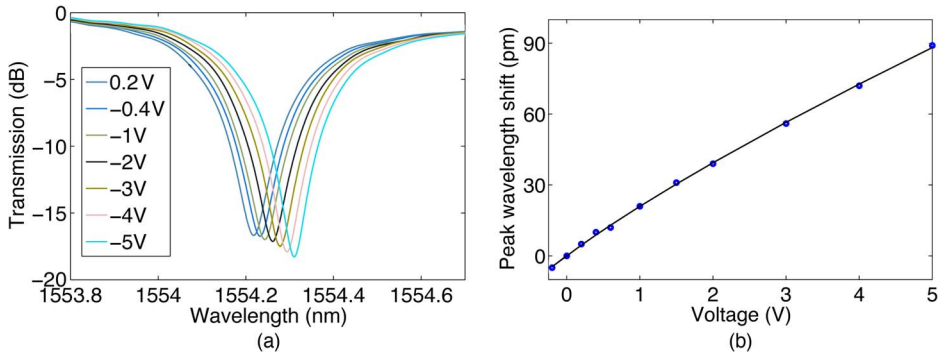


Fig. 4. PN junction tuning efficiency. (a) Spectra vs voltage. (b) Fitted peak shift vs voltage.

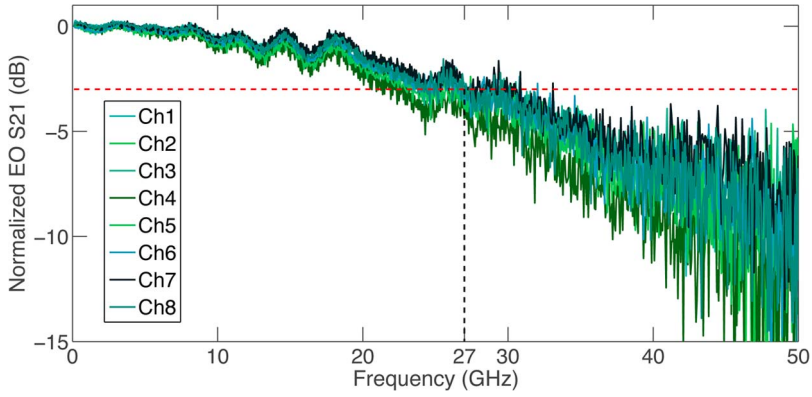


Fig. 5. Measured EO S21 of the 8 ring modulators in the WDM transmitter. Optical operating point is 6 dB below off-resonance level.

power of the ring resonator is 6 dB below its off-resonance level. This is the optical operating point that provides the sharpest slope for modulation [23]; therefore it is close to the condition that maximizes the optical modulation amplitude (OMA). In the data transmission measurements that will be discussed in later sections, we maintained similar offset from the resonance. At this "−6 dB" offset point, the modulation response peaking caused by intra-cavity dynamics is not significant but it still enhances EO bandwidth. The measured EO S21 traces from each of the 8 ring modulators in the WDM transmitter are shown in Fig. 5. The 8 ring modulators in the transmitter showed very similar bandwidth of around 27 GHz.

Overall, the ring modulator exhibits performance metrics comparable to the state-of-the-art in silicon using lateral pn junctions [24], while incorporated in-device thermal tuning. Better pn junction wavelength tunabilities can be achieved utilizing interdigitated junctions [25], [26], zigzag junctions [27] or vertical pn junctions with microdisk resonators [20], [28]. However, as discussed in [6], the improved tunability should be carefully traded off with a reduced modulation per capacitance as well as more complicated fabrication processes.

## 3. WDM Transmitter Design and Characterization

The WDM transmitter architecture was briefly discussed in Section 1. Fig. 1 shows the diagram and the photo of the fabricated device. In the WDM transmitter, the radii of the rings are designed to be slightly different so that the spacing between the resonance peak of two adjacent rings is 1.6 nm, i.e., an eighth of the FSR, in order to achieve cyclic operation with minimum tuning power. In the testing, grating couplers (GC) were used to couple laser on and off chip. A fiber array was attached to the silicon chip using epoxy, which made the optical coupling more stable during the testing. The

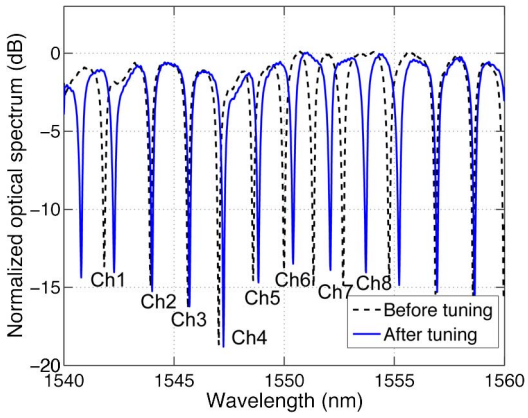


Fig. 6. Bus waveguide spectra before and after thermal tuning.

coupling loss per GC is estimated to be 5 dB. When the fiber-to-GC alignment is optimized, this loss can be reduced to approximately 3.5 dB. The overall on-chip insertion loss is 12 dB, including 0.9 dB from each ring modulator, and 5 dB due to unexpected high loss of 2 mm long routing waveguide covered by lower level metal interconnects. The 0.9 dB loss from the ring modulator is due to three main sources: the single-pass loss of the ring resonator, the loss due to the closely spaced directional coupler and the heavily doped thermal tuner in the coupler region. The latter two can be improved in future designs.

In the experiments, we first thermally tuned the 8 rings so that their resonance peaks were evenly distributed with the target 1.6-nm channel-spacing. The overall tuning power was 17 mW. The spectra before and after tuning is shown in Fig. 6. It is worth noting that before the tuning the 8 channels were already roughly evenly spaced owing to the pre-scaled ring radii and consistent dimensions of closely located devices. This helped reducing tuning power. Additional tuning power is required to align the resonance comb to a pre-defined laser wavelength grid in actual WDM systems. Because of the unidirectional nature of thermal tuning, the worst case scenario occurs when the comb is blue-shifted approximately one channel-spacing. Based on the thermal tuning efficiency, this entails 59 mW total tuning power. From a statistical standpoint [11], on average each ring only needs to be tuned a fraction ($\sim$60%) of one channel-spacing in a cyclic configuration, which implies 36 mW total tuning power in our design.

EO S-parameters characterize device bandwidth in small-signal regime and provide useful information that validates device design and modeling accuracy. The large-signal dynamic performance of the device in actual high-speed data transmission was evaluated by bit-error-rate (BER) versus optical signal-to-noise ratio (OSNR) measurements. Due to the high loss of the fiber coupling, erbium-doped fiber amplifiers (EDFA) needed to be inserted in the link in our experiments. Therefore, OSNR is used to characterize channel quality and to yield a fair comparison of the transmitters themselves. The experiment setup is shown in Fig. 7. Non-return-to-zero (NRZ) pseudo-random-bit-stream (PRBS) with $2^{31} - 1$ pattern at 10 Gb/s was generated by an Anritsu pulse pattern generator (PPG) and then 4-way split and delayed before being multiplexed into a 40 Gb/s bit-stream using an SHF 24210A module. The 40 Gb/s output was amplified by a Centellax OA4MVM3 driver amplifiers, then attenuated to the desired amplitude by passive attenuators. The driving signal was applied to the device through an high-speed bias-tee and a GS RF probe with 50 $\Omega$ in-probe termination. The terminated probe is to avoid large RF reflections that could damage the driver amplifier.

To operate each channel, a tunable continuous-wave (CW) laser was aligned to each of the evenly spaced resonance peaks with proper offset to reach the aforementioned $-6$ dB optical operating point. The modulated light was combined with tunable ASE noise loading that varied the OSNR in the experiments and then passed through an EDFA. The output optical signal was passed through an optical band-pass-filter with 6-nm bandwidth and then split into two branches. One

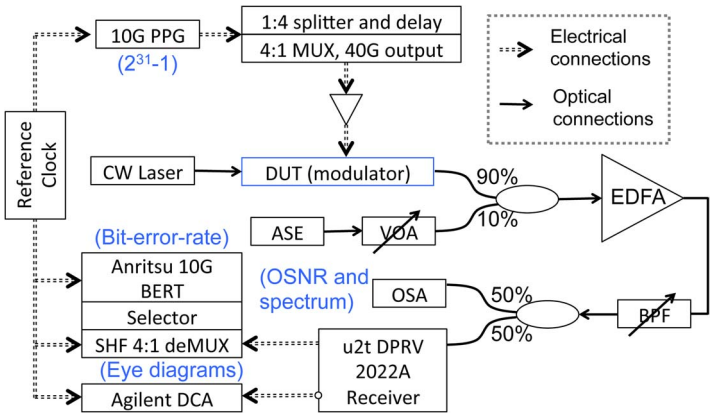


Fig. 7. Measurement setup for BER and eye-diagrams. (PPG: pulse pattern generator, VOA: variable optical attenuator, ASE: amplified spontaneous emission, BPF: optical bandpass filter, OSA: optical spectrum analyzer.)

branch was fed into an optical spectrum analyzer (OSA) for OSNR monitoring and the other was sent to a u2t DPRV 2022A receiver (AC coupled, $-10$ dBm sensitivity) with differential outputs. During the experiments the OMA into the receiver was maintained to be near 0 dBm, well above its sensitivity. One of the receiver output was connected to an Agilent 86100B digital communication analyzer (DCA) for capturing eye-diagrams. The other output was connected to an SHF 34210A 1 : 4 demultiplexer followed by an SHF 58210A selector. The demultiplexed and selected tributary was sent to an Anritsu MU181040A error-detector for BER test. The reported BER is an average of all 4 tributaries.

We carried out the BER versus OSNR measurement on each of the 8 channels in the silicon WDM transmitter and a commercial lithium niobate 40-Gb/s modulator that has 5.9 $V_\pi$ for comparison. The lithium niobate modulator is driven with 5.5 $V_{pp}$, which was the maximal available drive voltage from the driver amplifier due to limited output voltage from the multiplexer. The silicon ring modulator was tested with two different driving configurations: (1) "high drive": 4.8 $V_{pp}$ drive with 2.7 V reverse bias and (2) "low drive": 2.4 $V_{pp}$ drive with 1.1 V reverse bias. The device junction modulation power consumption can be calculated using $C_{pn}V_{pp}^2/4$ [29]. The two configurations correspond to 144 fJ/bit and 36 fJ/bit, respectively. For a complete transmitter, additional power is needed due to thermal tuning and driver circuits. At high data rates, with less advanced CMOS processes, driver circuits can consume more than an order of magnitude higher power compared to the power dissipated in charging and discharging the device capacitance [30]. However, with low-parasitic integration and advanced CMOS processes, CMOS inverter drivers have been demonstrated with under 100 fJ/bit [16]. In this case, an efficient modulator with low energy-per-bit is the key to improving overall power consumption.

The BER-OSNR measurement results are shown in Fig. 8. All of the 8 channels showed consistent performance with a OSNR penalty variation approximately 1.5 dB. On average, a 3.5-dB OSNR-penalty is observed between "high drive" ring modulator and lithium niobate modulator, and an additional 2.7-dB OSNR-penalty is observed between "high drive" and "low drive" cases. Because the receiver is AC coupled, an extinction ratio (ER) measurement was not readily available on the DCA. We measured the conversion gain of the receiver under various power levels and recorded the average power into the receiver in each experiment. Based on these measurements, we calculated that ER is 10 dB in the measurement of the lithium niobate modulator and the ER is 5 dB and 3 dB in WDM ring modulators with "high drive" and "low drive," respectively. We found that once we take into account the ER differences, the WDM ring modulators shows only 1.5–2 dB excess OSNR penalty. The excess OSNR penalty is attributed to ring modulator nonidealities, such as limited bandwidth, non-symmetric eye waveforms and etc. Incidentally, under "high drive" condition the test system had sufficient OSNR to reach error-free $(\text{BER} < 10^{-12})$. The error-free eye-diagrams were recorded and are presented in Fig. 9.

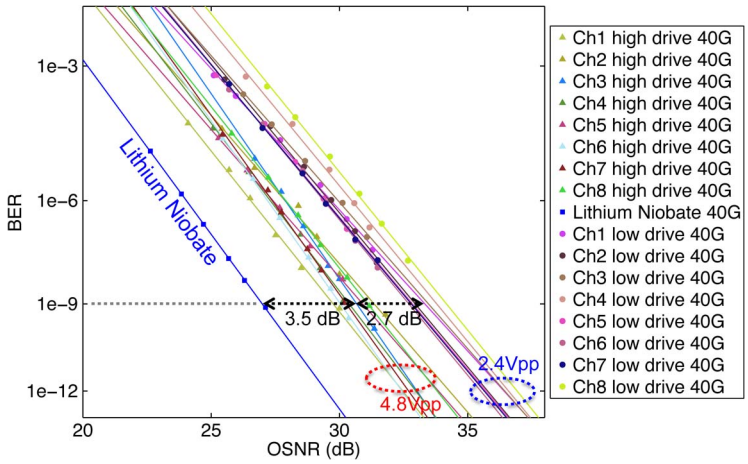


Fig. 8. BER measurements of reference lithium niobate modulator under 5.5 $V_{pp}$ drive and ring modulator under high-drive (4.8 $V_{pp}$) and low-drive (2.4 $V_{pp}$).

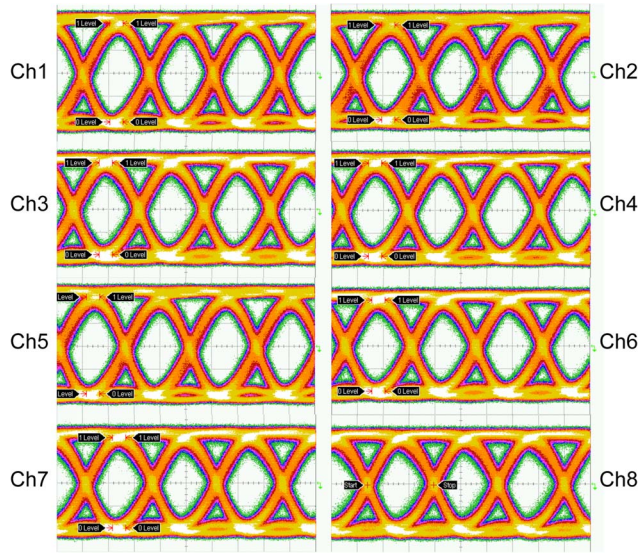


Fig. 9. Error-free $(\text{BER} < 10^{-12})$ eye-diagrams of 8-channels at full drive (4.8 $V_{pp}$) with 5 dB extinction ratio.

## 4. Conclusion

We report the design and characterization of an 8 $\times$ 40 Gb/s WDM transmitter in silicon. The transmitter is based on high-speed thermally-tunable ring modulators and achieves a compact footprint of 0.5 $mm^2$. The tuning power to achieve cyclic and evenly distributed wavelength channels is 17 mW. Owing to the small device capacitance of 25 fF and high pn-junction tunability of 25 pm/V, the transmitter demonstrates a low energy-per-bit of 36 fJ/bit at 40 Gb/s. All 8 channels showed consistent device characteristics as well as BER-OSNR performance and achieved error-free $(\text{BER} < 10^{-12})$ operation when given sufficient OSNR. To our knowledge, this work demonstrates the highest aggregated data rate in silicon WDM transmitters.

## Acknowledgment

The authors would like to thank G. Pomrenke, of AFOSR, for his support of the OpSIS effort. The authors gratefully acknowledge the loan of critical equipment for this project from AT&T. The

authors also thank Dr. N. Ophir, K. Padmaraju, and L. Zhu at Columbia University, New York, NY, USA, for their assistance with the high-speed measurements.

## References


[1] A. V. Krishnamoorthy *et al.,* "Computer systems based on silicon photonic interconnects," *Proc. IEEE*, vol. 97, no. 7, pp. 1337–1361, Jul. 2009.

[2] P. Dong *et al.,* "Monolithic silicon photonic integrated circuits for compact 100+ Gb/s coherent optical receivers and transmitters," *IEEE J. Sel. Topics Quantum Electron.*, vol. 20, no. 4, p. 6100108, Jul./Aug. 2014.

[3] A. Narasimha *et al.,* "A fully integrated 4 $\times$ 10-Gb/s DWDM optoelectronic transceiver implemented in a standard 0.13 $\mu$m CMOS SOI technology," *IEEE J. Solid-State Circuits*, vol. 42, no. 12, pp. 2736–2744, Dec. 2007.

[4] A. Liu *et al.,* "Wavelength division multiplexing based photonic integrated circuits on silicon-on-insulator platform," *IEEE J. Sel. Topics Quantum Electron.*, vol. 16, no. 1, pp. 23–32, Jan./Feb. 2010.

[5] L. Chen, C. R. Doerr, P. Dong, and Y.-K. Chen, "Monolithic silicon chip with 10 modulator channels at 25 Gbps and 100-GHz spacing," *Opt. Exp.*, vol. 19, no. 26, pp. B946–B951, Dec. 2011.

[6] G. Li *et al.,* "Ring resonator modulators in silicon for interchip photonic links," *IEEE J. Sel. Topics Quantum Electron.*, vol. 19, no. 6, p. 3401819, Nov./Dec. 2013.

[7] N. Ophir, C. Mineo, D. Mountain, and K. Bergman, "Silicon photonic microring links for high-bandwidth-density, low-power chip I/O," *IEEE Micro*, vol. 33, no. 1, pp. 54–67, Jan./Feb. 2013.

[8] P. Dong *et al.,* "Reconfigurable 100 Gb/s silicon photonic network-on-chip," presented at the Optical Fiber Commun. Conf., San Francisco, CA, USA, 2014, Paper Th4G.2. [Online]. Available: http://www.opticsinfobase.org/abstract.cfm?URI=OFC-2014-Th4G.2

[9] *Comb-Laser LD-1310-COMB-12*, Innolume, Dortmund, Germany, 2014. [Online]. Available: http://www.innolume.com/products/Comb-laser.htm

[10] X. Zheng *et al.,* "A 33 mW 100 Gbps CMOS silicon photonic WDM transmitter using off-chip laser sources," presented at the National Fiber Optic Engineers Conf., Anaheim, CA, USA, 2013, Paper PDP5C-9.

[11] A. V. Krishnamoorthy *et al.,* "Exploiting CMOS manufacturing to reduce tuning requirements for resonant optical devices," *IEEE Photon. J.*, vol. 3, no. 3, pp. 567–579, Jun. 2011.

[12] G.-D. Kim *et al.,* "Silicon photonic temperature sensor employing a ring resonator manufactured using a standard CMOS process," *Opt. Exp.*, vol. 18, no. 21, pp. 22 215–22 221, Oct. 2010.

[13] Q. Xu, B. Schmidt, J. Shakya, and M. Lipson, "Cascaded silicon micro-ring modulators for WDM optical interconnection," *Opt. Exp.*, vol. 14, no. 20, pp. 9431–9435, Oct. 2006.

[14] L. Chen, S. Manipatruni, and M. Lipson, "50 Gbit/s wavelength division multiplexing using silicon microring modulators," in *Proc. 6th IEEE Int. Conf. Group IV Photon.*, 2009, pp. 244–246.

[15] X. Xiao *et al.,* "60 Gbit/s silicon modulators with enhanced electro-optical efficiency," presented at the Optical Fiber Commun. Conf., Anaheim, CA, USA, 2013, Paper OW4J-3.

[16] X. Zheng *et al.,* "Ultralow power 80 Gb/s arrayed CMOS silicon photonic transceivers for WDM optical links," *J. Lightwave Technol.*, vol. 30, no. 4, pp. 641–650, Feb. 2012.

[17] A. Novack *et al.,* "A 30 GHz silicon photonic platform," in *Proc. SPIE Opt. Optoelectron.*, 2013, pp. 878107-1–878107-4.

[18] M. Gould, T. Baehr-Jones, R. Ding, and M. Hochberg, "Bandwidth enhancement of waveguide-coupled photodetectors with inductive gain peaking," *Opt. Exp.*, vol. 20, no. 7, pp. 7101–7111, Mar. 2012.

[19] M. Hochberg *et al.,* "Silicon photonics: The next fabless semiconductor industry," *IEEE Solid-State Circuits Mag.*, vol. 5, no. 1, pp. 48–58, Mar. 2013.

[20] E. Timurdogan *et al.,* "A one femtojoule athermal silicon modulator," in *arXiv preprint arXiv:1312.2683*, 2013.

[21] I.-L. Gheorma and R. Osgood, Jr., "Fundamental limitations of optical resonator based high-speed EO modulators," *IEEE Photon. Technol. Lett.*, vol. 14, no. 6, pp. 795–797, Jun. 2002.

[22] W. D. Sacher and J. K. Poon, "Dynamics of microring resonator modulators," *Opt. Exp.*, vol. 16, no. 20, pp. 15 741–15 753, Sep. 2008.

[23] H. A. Ayazi, "All-dielectric photonic-assisted radio front-end technology," Ph.D. dissertation, Univ. California, Los Angeles, CA, USA, 2011.

[24] G. Li *et al.,* "40 Gb/s thermally tunable CMOS ring modulator," in *Proc. IEEE 9th Int. Conf. GFP*, 2012, pp. 1–3.

[25] M. Ziebell *et al.,* "Ten Gbit/s ring resonator silicon modulator based on interdigitated PN junctions," *Opt. Exp.*, vol. 19, no. 15, pp. 14 690–14 695, Jul. 2011.

[26] J. Rosenberg *et al.,* "A 25 Gbps silicon microring modulator based on an interleaved junction," *Opt. Exp.*, vol. 20, no. 24, pp. 26 411–26 423, Nov. 2012.

[27] X. Xiao *et al.,* "25 Gbit/s silicon microring modulator based on misalignment-tolerant interleaved PN junctions," *Opt. Exp.*, vol. 20, no. 3, pp. 2507–2515, Jan. 2012.

[28] M. R. Watts, W. A. Zortman, D. C. Trotter, R. W. Young, and A. L. Lentine, "Vertical junction silicon microdisk modulators and switches," *Opt. Exp.*, vol. 19, no. 22, pp. 21 989–22 003, Oct. 2011.

[29] P. Dong *et al.,* "Low$V_{pp}$, ultralow-energy, compact, high-speed silicon electro-optic modulator," *Opt. Exp.*, vol. 17, no. 25, pp. 22 484–22 490, Dec. 2009.

[30] J. F. Buckwalter, X. Zheng, G. Li, K. Raj, and A. V. Krishnamoorthy, "A monolithic 25-Gb/s transceiver with photonic ring modulators and Ge detectors in a 130-nm CMOS SOI process," *IEEE J. Solid-State Circuits*, vol. 47, no. 6, pp. 1309–1322, Jun. 2012.